Atmos. Meas. Tech. Discuss., 7, 3801–3833, 2014
www.atmos-meas-tech-discuss.net/7/3801/2014/
doi:10.5194/amtd-7-3801-2014

Atmospheric Measurement Techniques Discussions
Open Access

Aircraft validation of Aura Tropospheric Emission Spectrometer retrievals of HDO and H_2O

R. L. Herman[1], J. E. Cherry[2,3], J. Young[2], J. M. Welker[4], D. Noone[5,6], S. S. Kulawik[7], and J. Worden[1]

[1]Jet Propulsion Laboratory, California Institute of Technology, Pasadena, California, USA
[2]International Arctic Research Center, University of Alaska Fairbanks, Alaska, USA
[3]Institute of Northern Engineering, University of Alaska Fairbanks, Alaska, USA
[4]Department of Biological Sciences, University of Alaska Anchorage, Alaska, USA
[5]Department of Atmospheric and Oceanic Sciences, University of Colorado at Boulder, Boulder, Colorado, USA
[6]Cooperative Institute for Research in Environmental Sciences, University of Colorado at Boulder, Boulder, Colorado, USA
[7]Bay Area Environmental Research Institute, Mountain View, California, USA

Received: 3 March 2014 – Accepted: 21 March 2014 – Published: 14 April 2014

Correspondence to: R. L. Herman (robert.l.herman@jpl.nasa.gov)

Published by Copernicus Publications on behalf of the European Geosciences Union.

Abstract

The EOS Aura Tropospheric Emission Spectrometer (TES) retrieves the atmospheric HDO/H_2O ratio in the mid-to-lower troposphere as well as the planetary boundary layer. TES observations of water vapor and the HDO isotopologue have been compared with nearly coincident in situ airborne measurements for direct validation of the TES products. The field measurements were made with a commercially available Picarro L1115-i isotopic water analyzer on aircraft over the Alaskan interior boreal forest during the three summers of 2011 to 2013. TES special observations were utilized in these comparisons. The TES averaging kernels and a priori constraints have been applied to the in situ data, using Version Five (V005) of the TES data. TES calculated errors are compared with the standard deviation ($1-\sigma$) of scan-to-scan variability to check consistency with the TES observation error. Spatial and temporal variations are assessed from the in situ aircraft measurements. It is found that the standard deviation of scan-to-scan variability of TES δD is ±34.1 ‰ in the boundary layer, and ±26.5 ‰ in the free troposphere. This scan-to-scan variability is consistent with the TES estimated error (observation error) of 10–18 ‰ after accounting for the atmospheric variations along the TES track of ±16 ‰ in the boundary layer, increasing to ±30 ‰ in the free troposphere observed by the aircraft in situ measurements. We estimate that TES V005 δD is biased high by an amount that decreases with pressure: approximately +12.3 % at 1000 hPa, +9.8 % in the boundary layer, and +3.7 % in the free troposphere. The uncertainty in this bias estimate is ±2 %. After bias correction, we show that TES has accurate sensitivity to water vapor isotopologues in the boundary layer.

1 Introduction

The isotopic composition of water vapor is useful for characterizing the processes, sources, and sinks controlling water in the atmosphere (e.g., Craig, 1961; Dansgaard, 1964). Evaporation from bodies of liquid water is a fractionating process with depleted

AMTD

7, 3801–3833, 2014

Aircraft validation of TES HDO and H_2O

R. L. Herman et al.

HDO/H_2O in the gas phase. This water vapor is transported horizontally by advection, and vertically by convection within the boundary layer. Over land, water vapor enters the atmosphere by transport, evaporation and plant transpiration, each of which have different fractionation pathways. Condensation and precipitation preferentially remove the heavier HDO isotopologue from the gas phase. Permanent removal of precipitation from an unmixed air parcel leads to Rayleigh distillation, leaving increasingly depleted HDO/H_2O in the gas phase. Evaporation of precipitation at lower altitudes in the atmosphere can enrich HDO/H_2O in the gas phase (e.g., Worden et al., 2007; Noone, 2012), and is related to the "amount" effect described by Dansgaard (1964). Collectively these physical and biological processes impart an integrated isotopic fractionation of water vapor in the atmosphere, thus providing useful information about the intensity of the hydrologic cycle (important to climate studies), transport and mixing processes in the atmosphere, and sources of atmospheric moisture (e.g., local vs. distant, convection vs. evapotranspiration).

Spaceborne instruments that measure isotopologues of water vapor, such as the Aura Tropospheric Emission Spectrometer (TES), provide regional constraints on the hydrologic cycle. As reported by Worden et al. (2007), the isotopic composition of tropospheric water vapor may differ significantly from the isotopic composition of precipitation due to separate sources. Therefore, remote sensing provides new information about the hydrologic cycle unattainable from water measurements at the surface. Water vapor isotopic measurements from TES have improved our understanding of the hydrologic cycle in the Tropics (Worden et al., 2007; Noone, 2012), Hawaii (e.g. Noone et al., 2011), the Amazon rainforest (Brown et al., 2008), and the Asian and North Australian monsoon (e.g., Brown et al., 2008; Lee et al., 2011). These studies principally rely on the precision of space-based measurements, but they also call for accurate measurements that are tied to the international absolute scale, and therefore require that remotely sensed data be carefully calibrated against complementary measurements with well-characterized accuracy.

Discussion Paper | Discussion Paper | Discussion Paper | Discussion Paper |
AMTD
7, 3801–3833, 2014

Water isotopologues have been measured from space in the mid-infrared region of the electromagnetic spectrum. First were measurements of the upper troposphere and lower stratosphere (UTLS), pioneered by the ATMOS (Atmospheric Trace Molecule Spectroscopy) mission on the Space Shuttle (Rinsland et al., 1991; Irion et al., 1996; Moyer et al., 1996; Kuang et al., 2003) over limited geographical locations. Extensive UTLS measurements of HDO and H_2O were introduced by the IMG (Interferometer for Monitoring of Greenhouse Gases) on the ADEOS-1 (Advanced Earth Observing Satellite) platform (Zakharov et al., 2004; Herbin et al., 2007). More recent stratospheric HDO observations have been provided by Envisat/MIPAS (Michelson Interferometer for Passive Atmospheric Sounding) (Steinwagner et al., 2010, 2007), Odin/SMR (Sub-Millimetre Radiometer) (Murtagh et al., 2002; Urban et al., 2007), and SCISAT/ACE-FTS (Atmospheric Chemistry Experiment – Fourier Transform Spectrometer) (Bernath et al., 2005; Randel et al., 2012). Ground-based remote sensing by the FTIR technique has retrieved atmospheric HDO and H_2O profiles (Schneider et al., 2006, 2010). Tropospheric HDO and H_2O, the topic of this paper, have been measured from space by Envisat/SCIAMACHY (Scanning Imaging Absorption Spectrometer for Atmospheric Chartography) (Frankenberg et al., 2009), IASI (Infrared Atmospheric Sounding Interferometer) aboard the MetOp satellites (Herbin et al., 2009; Schneider and Hase, 2011; Lacour et al., 2012), and Aura TES (Worden et al., 2006, 2007).

EOS Aura was launched into orbit on 15 July 2004 to study atmospheric chemistry (Schoeberl et al., 2006; http://aura.gsfc.nasa.gov/) and to complement EOS Aqua as part of the A-Train constellation of Earth observing satellites. In Version Five (hereafter V005) retrievals, HDO and H_2O are measured by Aura TES with the greatest sensitivity in the mid-to-lower troposphere and the boundary layer. What sets this version apart from earlier versions of TES data is enhanced sensitivity to the lower troposphere with the capability to distinguish the isotopic composition of the lower troposphere from the mid-troposphere due to the substantially increased number of HDO spectral lines used in the TES HDO/H_2O retrieval (Worden et al., 2012). The focus of this paper is

AMTD
7, 3801–3833, 2014

Aircraft validation of TES HDO and H_2O

R. L. Herman et al.

validation of the new TES HDO/H_2O isotopic abundances with airborne in situ measurements.

2 TES retrievals

2.1 TES instrument description

TES provides global vertically-resolved measurements every two days of ozone, carbon monoxide, HDO and H_2O, temperature, and a number of other atmospheric chemical species that are critical to tropospheric air pollution studies (Beer, 2006). TES is an infrared, high-resolution imaging Fourier Transform Spectrometer that covers a spectral range of 650 to 3050 cm^{-1} at 0.1 cm^{-1} spectral resolution in the nadir view (Beer et al., 2001; Beer, 2006). This paper focuses exclusively on TES special observation retrievals in the nadir-viewing mode, which have a footprint of 5.3 km by 8.4 km (see Sect. 3.1 for details on special observations). In nadir and off-nadir retrievals, height discrimination is provided by spectral resolution of pressure-broadened wings at higher pressures and linecenter features at lower pressures (Beer et al., 2002). TES retrievals use the optimal estimation method to quantify atmospheric species (Rodgers, 2000). The algorithms and spectral microwindows are described by Worden et al. (2004, 2006, 2011, 2012) and Bowman et al. (2002, 2006). The standard Level 2 data products are written in HDF-EOS5 format (based on HDF5), and are publically available from the NASA Langley Atmospheric Science Data Center (ASDC): https://eosweb.larc.nasa.gov/project/tes/tes_table with V005 files ending in “F06_07”, “F06_08”, or “F06_09.” Alternatively, the “Lite Product” has smaller files written in NetCDF format, and is publically available from the NASA Aura Validation Data Center (AVDC): http://avdc.gsfc.nasa.gov. Existing TES data at these sites are designated by Earth Science Data Type V005.

AMTD
7, 3801–3833, 2014

2.2 TES joint retrieval

One of the most important new features of TES V005 data is the joint retrieval of water vapor, HDO, N_2O and CH_4 (Worden et al., 2012). The entire spectral region between 1170 and 1330 cm^{-1} is used to jointly estimate H_2O, HDO, CH_4, and N_2O. This has several benefits, including greater resolution of water vapor in the lower troposphere (Herman et al., 2013), and higher degrees of freedom for signal (hereafter DOFS) for HDO.

The initial guess in the TES retrieval algorithm is set equal to an a priori profile (constraint vector). For the water vapor parent molecule $H_2{}^{16}O$, the TES a priori constraint vectors come from NASA's Goddard Earth Observing System (GEOS) data assimilation system GEOS-5.2 (Rienecker et al., 2007). These are produced by the Global Modeling and Assimilation Office (GMAO) at the NASA Goddard Space Flight Center (GSFC). GEOS-5.2 assimilates a wide range of data from operational satellites, radiosondes, and other sources. Radiosonde data are strong constraints on the thermal structure and winds throughout the troposphere, with an emphasis on continental regions where the observing network is denser. Space-based observations include the High Resolution Infrared Sounders (HIRS) and Advanced Microwave Sounders (AMSU) instruments on NOAA's operational sounders, which directly constrain temperature and moisture. GEOS-5 includes a direct assimilation of radiances from AMSU and HIRS in a three-dimensional variational assimilation, as well as radiances from the Advanced Infrared Sounder (AIRS) and AMSU instruments on NASA's EOS-Aqua platform (Zhu and Gelaro, 2007). GMAO GEOS-5.2 water vapor fields are produced on a 0.625° longitude by 0.5° latitude grid with 36 pressure levels and 6 h temporal resolution. These are interpolated to the locations and pressure levels of TES retrievals. For all retrievals, a priori HDO is defined as the product of the local a priori H_2O profile (GMAO GEOS-5.2) and one tropical a priori profile of the HDO/H_2O isotopic ratio (Worden et al., 2006).

AMTD
7, 3801–3833, 2014

Validating the accuracy of TES HDO and H_2O retrievals is important for studies of the hydrologic cycle, exchange processes in the troposphere, and climate change. Worden et al. (2011) performed validation comparisons of the previous version (V004) TES HDO/H_2O data with in situ measurements at Mauna Loa, Hawaii, and concluded that TES V004 δD data are biased high by 6.3 ± 1.9 % (i.e., 63 ± 19 ‰). In this paper, we denote the volume mixing ratios q_D for HDO, and q_H for H_2O. By standard convention, we report the isotopic abundance as δD (per mil or ‰) $= [(q_D/q_H)_{obs}/(q_D/q_H)_{std} - 1] \times 1000$, where $(q_D/q_H)_{std} = 3.11 \times 10^{-4}$ based on the D/H standard ratio for Vienna Standard Mean Ocean Water. In Sect. 4.3 below, we characterize the new bias estimate for TES V005 δD.

3 Data

3.1 TES data

TES special observations are scheduled for coordinated validation missions or special atmospheric features of interest to the TES science team. In this paper, the focus is transect special observations scheduled over Alaska during the summers of 2011 to 2013 for coordination with aircraft measurements of HDO and H_2O (see Sect. 3.2 below for Aircraft Data). The transect is a series of twenty consecutive scans spaced 12 km apart for dense geophysical coverage of retrievals. Transects are most useful for comparison to aircraft, which can fly along the satellite track to spatially overlap with multiple satellite scans. The much faster ground speed of the satellite than the aircraft means that only one observation will be coincident in time. The other observations are very close in time: the total duration of a transect is approximately 216 s. This implies that, for the set of twenty scans within a TES transect, the observed variance of the TES retrievals is more influenced by spatial heterogeneity ($\leq$ 240 km distance) than by temporal differences over this short timeframe. In these twenty scans, the TES geolocations are oriented along a line parallel to the sub-satellite track. TES transects have

AMTD
7, 3801–3833, 2014

been programmed to point either nadir or slightly off-nadir, depending on the location of the target relative to the sub-satellite track. One advantage of the transect is that atmospheric variability can be assessed on a scale of tens of kilometers. In the case of aircraft comparisons, the topic of this paper, the aircraft is flown along the transect ground track to maximally overlap with the Aura overpass.

3.2 Aircraft data

The University of Alaska, Fairbanks, team provided in situ measurements on board a Navion L-17a aircraft. Air was sampled into the aircraft through an inlet probe with flow provided by the ram pressure as the aircraft flew. Meteorological parameters (outside air temperature, relative humidity, and barometric pressure) were provided by a commercial Vaisala HMT307 sensor. Water vapor isotopic abundances (HDO/H_2O and $H_2{}^{18}O/H_2{}^{16}O$) were measured in situ with a commercial Picarro L1115-i $\delta D/\delta^{18}O$ Ultra High-Precision Isotopic Water Analyzer using the cavity ring-down (CRD) spectroscopic technique (O'Keefe and Deacon, 1988; Berden et al., 2000; Gupta et al., 2009). The bench performance of this particular Picarro unit was measured by the manufacturer as follows: the precision ($1-\sigma$) of δD was 0.0363 ‰ for 30 s averaging time and 8000 parts per million by volume (ppmV) water vapor (A. Van Pelt, personal communication, 2014).

In contrast to bench measurements, airborne measurements were susceptible to a number of factors that may introduce error, including rapidly changing pressure, temperature, and water vapor. Atmospheric profiles of in situ δD were obtained by changing altitude of the aircraft. On many of the aircraft flights in 2011 and 2012, hysteresis was observed between aircraft ascent and descent isotopic measurements. Upon rapid descent, δD data were consistently more isotopically depleted than the ascent data, and atmospheric layers appeared at lower altitudes than the ascent data due to instrument time response issues. Aircraft testing in 2013 revealed that slower climb/descent rates yielded more consistent δD measurements. For the 2011–2012 flights, we use only the ascent data due to slower climb rates and extensive duration at the same

Discussion Paper | Discussion Paper | Discussion Paper | Discussion Paper |
AMTD
7, 3801–3833, 2014
Aircraft validation of TES HDO and H_2O
R. L. Herman et al.

altitude in stair-step flight patterns (Fig. 1). Additionally, error increased near the ground due to heterogeneous vegetation and topography, and near atmospheric wind shear zones. To minimize error, isotopic standards were injected in-flight at various altitudes while flying in level circles. We conservatively estimate the practical "in-field" error of δD to be ±4 ‰ for 5 s averaging time.

3.3 Method of comparison

Following the approach of Rodgers and Connor (2003), satellite and in situ data may be compared directly if the satellite averaging kernel is applied to the in situ data to treat both atmospheric profiles with the same vertical sensitivity. Aircraft in situ measurements have a much finer vertical resolution than satellite retrievals. The TES operator, which consists of the a priori constraint x_a and the TES averaging kernel matrix $\mathbf{A}$, is used to smooth the in situ data to the same resolution as the satellite retrievals. TES retrievals are performed on the logarithm of the volume mixing ratios, $x_D = \ln(q_D)$ and $x_H = \ln(q_H)$. Worden et al. (2006) have described in detail how the TES operator is applied to in situ measurements. In short, the in situ data are interpolated to a very fine grid. Above the aircraft maximum altitude, the profile is extrapolated using a scaled a priori profile (see Sect. 4.4 for details). The entire profile is mapped onto the standard pressure levels to give the profile x. The TES operator is used according to the following relation:

$$x_{\mathrm{insituw/AK}} = x_a + \mathbf{A}(x - x_a) \quad (1)$$

to calculate $x_{\mathrm{insituw/AK}}$, the in situ profile with applied averaging kernel and a priori constraint. In this paper, all comparisons have been completed using the TES operator.

To minimize the impact of atmospheric spatial and temporal variability, satellite and aircraft measurements were selected for close coincidence. For the direct comparisons, only measurements within ±1 h were included, for TES scans that are within 12 km of the aircraft path (see Table 1). For all HDO retrievals, the initial profile of the $HDO/H_2{}^{16}O$ isotopic ratio is set equal to a simulated tropical profile (Worden et al.,

Discussion Paper | Discussion Paper | Discussion Paper | Discussion Paper

AMTD

7, 3801–3833, 2014

Aircraft validation of TES HDO and H_2O

R. L. Herman et al.

2006). The standard data retrieval quality flags are used in this analysis, as outlined in the TES L2 Data User's Guide, version 5.0 (Herman and Kulawik, 2013). Following Worden et al. (2007) and Brown et al. (2008), we filter data for a reasonable threshold of DOFS (DOFS > 1.1), but include all cloud optical depths. As seen in Table 1, several of the comparison dates had nearly clear-sky conditions.

4 Analysis

4.1 Atmospheric variability

The in situ aircraft isotopic measurements allow us to characterize the error in the true profile of HDO/H_2O. Data from seven aircraft flights over the Alaskan boreal forest were binned by TES pressure level, with statistics shown in Table 2. As mentioned in Sect. 3.2, hysteresis was observed between aircraft ascent and descent, so only the ascent data are considered here. The top of the boundary layer over the boreal forest was typically between 1.2 and 2.0 km elevation above sea level (a.s.l.), corresponding to a pressure range of 900 to 790 hPa. The isotopic ratio of HDO/H_2O is generally uniform within the boundary layer, and less isotopically depleted than in the free troposphere. The mean δD of boundary layer water vapor measured by seven aircraft flights is equal to −230 ‰, and the standard deviation ($1-\sigma$) of δD is ±16 ‰. The boundary layer statistics for each individual flight are shown in Table 2. In the free troposphere, HDO/H_2O is more isotopically depleted than in the boundary layer, and shows greater variability: the standard deviation ($1-\sigma$) of δD is ±30 ‰. This variability is much larger than the Picarro instrument precision, and is due to transport of water vapor and the processes of condensation and precipitation.

The variance of TES retrieved δD is influenced by both atmospheric variability and the error of the TES retrieval. As a first step toward characterizing the error budget of TES δD retrievals, we examine the scan-by-scan variability within single TES transect special observations over the Alaskan interior boreal forest. To optimize for clear-sky

AMTD
7, 3801–3833, 2014

and warm conditions, only measurements from July and August (2011–2013) are considered here. This corresponds to 27 Alaskan interior transects, and a total of 253 TES scans with DOFS greater than 1.1. Figure 2 shows the mean δD and standard deviation of δD for each transect (black), and the overall average (thick red line). At the near-surface pressure level, the TES retrieval is somewhat influenced by the prior. This is also true at altitudes above 10 000 m. The standard deviation of δD has two peaks around 2000 m altitude (826 and 909 hPa pressure levels) and 8000 m altitude (422 and 464 hPa pressure levels) because the peak variability also corresponds to the levels with peak TES sensitivity to HDO/H_2O. The overall mean δD and standard deviation of δD are shown in bold red lines in Fig. 2, and also listed in Table 3. Scan-to-scan variability in these TES retrievals is characterized by the standard deviation of δD ($1-\sigma$), which is ±34.1 ‰ in the boundary layer (averaging the data from 826 and 909 hPa pressure levels), and ±26.5 ‰ in the free troposphere (averaging data from 750 to 383 hPa pressure levels). This analysis excludes the 1000 hPa pressure level, and pressures less than 383 hPa, due to decreased TES sensitivity to HDO at lower pressures (i.e., more influenced by the prior). The concentration of HDO drops with increasing altitude in the atmosphere due to three factors: decreasing pressure, drier air, and more isotopically depleted δD.

4.2 Comparison of TES with aircraft measurements

In this section, we show one representative comparison between TES and aircraft HDO measurements. Figure 3 shows the comparison between aircraft water vapor δD from the aircraft flight of 28 July 2012 and the coincident TES retrieval (Run 15 143, Scan 12). First, the aircraft ascent δD is interpolated to the TES pressure levels (red diamonds in Fig. 3a). The near-surface point is extrapolated from the aircraft data on the assumption that the boundary layer is well-mixed. The TES operator consisting of averaging kernel and prior from Eq. (1) is applied to the mapped in situ data. This allows a comparison between the mapped in situ data (red line in Fig. 3b) and TES (black line in Fig. 3b) that accounts for the a priori bias and sensitivity of the satellite retrieval

(Rodgers and Connor, 2003). The tropical prior (dash dot dot line in Fig. 3b) has significantly less depleted δD than either aircraft or TES because it is not representative of the isotopic abundance at high latitudes. Figure 3c shows the TES HDO averaging kernels for this TES scan. Finally, Fig. 3d shows a similar comparison for H_2O, where the TES operator is applied to the aircraft water vapor measurements. It is seen that TES has much finer vertical resolution for H_2O than HDO/H_2O. This is not surprising considering the higher DOFS for H_2O and the relative scarcity of HDO. Nevertheless, Fig. 3b shows that TES δD in the free troposphere has a similar profile as the in situ data with averaging kernel applied. Furthermore, TES provides some information about δD in the boundary layer. Otherwise, the TES δD profile would completely revert to the a priori value.

4.3 TES Bias correction

As reported in Worden et al. (2006, 2007, 2011), TES HDO/H_2O ratios are biased compared to model and in situ measurements. The source of this bias is assumed to be biases in spectroscopic line strengths. To properly account for the sensitivity of the TES retrieval, we use a bias correction based on Worden et al. (2011) Eq. (1):

$$\ln\left(\hat{q}^{\mathrm{D}}_{\mathrm{corrected}}\right) = \ln\left(\hat{q}^{\mathrm{D}}_{\mathrm{original}}\right) - \mathbf{A}_{\mathrm{DD}}\boldsymbol{\delta}_{\mathrm{bias}} \tag{2}$$

where $\hat{q}^{\mathrm{D}}_{\mathrm{original}}$ is the HDO volume mixing ratio estimate from the TES product files, $\mathbf{A}_{\mathrm{DD}}$ is the averaging kernel matrix from the product files, and $\boldsymbol{\delta}_{\mathrm{bias}}$ is a column vector of the fractional bias correction to $\hat{q}^{\mathrm{D}}_{\mathrm{original}}$ (not to be confused with δD notation). Since one cannot distinguish between spectroscopic uncertainties in HDO or H_2O, the bias is aggregated into the HDO bias.

Figure 4 shows the difference between TES and in situ δD for all coincident measurements. The bias column vector $\boldsymbol{\delta}_{\mathrm{bias}}$ was adjusted to minimize the difference between bias-corrected TES and in situ δD with TES operator applied. The comparison in Fig. 4

AMTD
7, 3801–3833, 2014

uses a linear relation to approximate the TES bias:

$$\delta_{\text{bias}} = 0.00019 \times \text{Pressure} - 0.067 \quad (3)$$

This corresponds to a typical TES bias of +9.8 % in the boundary layer (average for 909 and 825 hPa pressure levels), and +3.7 % in the free troposphere (average for 750 to 383 hPa pressure levels).

4.4 Assumptions about sensitivity to the true profile

The aircraft ceiling on these validation flights was between 3 and 5 km a.s.l. (see Table 1). This complicates comparisons because TES has greatest sensitivity to HDO/H_2O at two levels, one overlapping with the aircraft (2 km a.s.l.) the other above the aircraft (6 km a.s.l.). In order to apply the averaging kernel, the "true" HDO/H_2O ratio must be extrapolated above the aircraft measurements. To determine the sensitivity of the results to the "true" profile, we have applied two different assumptions. Figure 4 shows comparisons between TES and the best estimate of the "true" profile with averaging kernel. In this default case, the "true" profile consists of two segments: aircraft data in the lower troposphere, and a scaled prior at altitudes above the aircraft measurements. The prior HDO/H_2O profile is scaled by a constant factor so that the ratio at the TES level nearest the aircraft ceiling matches the aircraft HDO/H_2O. The prior HDO/H_2O is scaled by the constant factor from the aircraft ceiling up to the tropopause. An unscaled prior is used above the tropopause. Results are not sensitive to assumptions about the "true" profile above the tropopause because TES does not have much sensitivity to HDO at those levels.

For sensitivity testing, the "true" profile is varied as follows. The profile consists of aircraft data in the lower troposphere, and the scaled prior ±30 ‰ between the aircraft ceiling and the level where this intercepts the unscaled prior. Figure 5 shows the comparisons for these cases (scaled prior ±30 ‰). It is seen that the effect of changing the "true" profile is a change in TES bias, especially at 6000 to 8000 m altitude (corresponding to TES pressure levels 464 to 348 hPa). At these altitudes, a ±30 ‰ change

AMTD
7, 3801–3833, 2014

in the "true" profile corresponds to a ±20 ‰ or 2 % change in δD if the TES operator is applied.

5 Error estimation

The optimal estimation method allows characterization of the TES error budget (Worden et al., 2004, 2006; Bowman et al., 2004; Rodgers, 2000). One of the important uses of the correlative aircraft data is to assess this error budget. In the general case, the error $\tilde{x}$ in the estimate of the atmospheric profile is the difference between the true state x and the linear estimate $\hat{x}$ retrieved by TES (Worden et al., 2006, Eq. 15):

$$\tilde{x} = x - \hat{x}. \tag{4}$$

In Eq. (5) below, we define a term, the *estimated error* of the TES isotopic ratio HDO/H_2O, based on the theoretical expected error derived from optimal estimation retrieval theory. If the TES operator is applied to the in situ measurements, then the estimated error does not include smoothing error. In this case, where we compare TES and the aircraft measurements with averaging kernel, the estimated error covariance is given by the observation error covariance (Worden et al., 2006):

$$\mathbf{S} = \mathbf{G}_\mathrm{R}\mathbf{S}_\mathrm{n}\mathbf{G}_\mathrm{R}^\mathrm{T} + \mathbf{G}_\mathrm{R}\left(\sum_i \mathbf{K}_i\mathbf{S}_\mathrm{b}^i\mathbf{K}_i^\mathbf{T}\right)\mathbf{G}_\mathrm{R}^\mathrm{T}, \tag{5}$$

where the gain matrix $\mathbf{G}_\mathrm{R} = \left(\mathbf{G}_\mathrm{z}^\mathrm{D} - \mathbf{G}_\mathrm{z}^\mathrm{H}\right)$, $\mathbf{S}_\mathrm{n}$ is the measurement error covariance, and $\mathbf{S}_\mathrm{b}^i$ is the error covariance due to all other parameters, trace gases, temperature, et cetera, that affect the retrieval. The first term in Eq. (5) is the measurement error, and the second term is the sum of all systematic and interference error terms. Both measurement error and observation error covariance matrices are provided in the TES HDO Lite Product file. The estimated error is given by the square roots of the diagonal elements of $\mathbf{S}$, the best estimate of the TES observation error covariance for the HDO/H_2O retrieval.

In this section we define two additional figures of merit for error estimation of the isotopic ratio. On each TES retrieval pressure level, bias $\Delta_{\text{TES-AC}}$ is defined as the mean difference between the TES estimate $(\hat{q}_D/\hat{q}_H)$ and the aircraft isotopic ratio with averaging kernel applied, $(q_D/q_H)_{\text{insituw/AK}}$:

$$\Delta_{\text{TES-AC}} = \frac{1}{n}\sum_{i=1}^{n}\left[(\hat{q}_D/\hat{q}_H) - (q_D/q_H)_{\text{insituw/AK}}\right]_i \quad (6)$$

for n matched TES-aircraft pairs of observations. For consistency, we convert this bias to δD notation in all figures and tables. Empirical error is defined as the measured scan-to-scan variability quantified as the standard deviation of the difference between the TES estimate and the aircraft isotopic ratio:

$$\text{Empirical error} = \sqrt{\left(\frac{1}{n-1}\right)\sum_i \left\{\left[(\hat{q}_D/\hat{q}_H) - (q_D/q_H)_{\text{insituw/AK}}\right]_i - \Delta_{\text{TES-AC}}\right\}^2}. \quad (7)$$

Figure 6 is a comparison for a single match (28 July 2012) between TES HDO/H_2O observation error (red dashed line) and the empirical error (solid black line) plotted as fractional error in HDO/H_2O. It is seen that the empirical error is larger than the observation error. In the boundary layer, 1000 to 825 hPa, the empirical error is 0.029 (corresponding to ± 26 ‰ error in δD) and the observation error is 0.017 (corresponding to ±16 ‰ error in δD). In the lower troposphere, 750 to 681 hPa pressure levels, the errors have local minima. Here, the empirical error is 0.025 (corresponding to ±22 ‰ error in δD) and the observation error is 0.012 (corresponding to ±10.5 ‰ error in δD). At higher altitudes, there is a second peak in observation error comparable to the BL peak. The empirical error is significantly higher due to uncertainties in the true profile above the aircraft ceiling, which was 4.4 km or 585 hPa on 28 July 2012. Another reason for higher empirical error is natural atmospheric variability along the TES transect. As described above in Sect. 4.1, the aircraft measured atmospheric variability of ±16 ‰ in the boundary layer, increasing to ±30 ‰ in the free troposphere.

6 Discussion and summary

HDO/H_2O estimates from TES V005 retrievals over the Alaskan interior boreal forest have been compared to coincident in situ airborne measurements made with a Picarro Isotopic Water Analyzer. We have shown that TES V005 retrievals have sensitivity to HDO in the mid-to-lower troposphere and the boundary layer. From comparison with the aggregate of TES/in situ comparisons, we estimate that TES V005 δD should be corrected downwards by column vector $\boldsymbol{\delta}_{\text{bias}}$ (Eq. 3). This amounts to a net bias correction of −9.8 % in the boundary layer, decreasing to approximately −3.7 % in the free troposphere. The uncertainty in the bias correction is estimated to be 2 %. TES V005 HDO and H_2O are sufficiently accurate to be applied to studies of atmospheric water sources (e.g., transpiration, evaporation, precipitation, transport).

The error budget for Aura TES V005 HDO/H_2O is summarized in Table 4. In the Alaskan Boreal forest, the mean boundary layer δD is −230 ± 16 ‰ based on in situ aircraft measurements. The variability of in situ δD increases to approximately ±30 ‰ (1−σ st. dev.) in the free troposphere. There is greater variability in the free troposphere than in the boundary layer due to transport of HDO/H_2O. From analysis of twenty seven TES transects over the Alaskan boreal forest, the scan-to-scan variability of δD is ±34.1 ‰ in the boundary layer (averaging the data from 825 and 909 hPa pressure levels), and ±26.5 ‰ in the free troposphere (750 to 383 hPa pressure levels). From matched TES-aircraft pairs of observations, we estimate the TES empirical error (1 − σ st. dev.) to be ±26 ‰ in the boundary layer, and ±22 ‰ in the free troposphere below the ceiling of the aircraft measurements (see Sect. 5). The scan-to-scan TES variability is larger than the TES empirical error for a couple reasons: the scan-to-scan variability was calculated from all transect scans with good quality, not just the ones within 12 km of the aircraft, and some of these transects were on aircraft "no-fly" days with inclement weather. From the HDO/H_2O observation error, the TES estimated error is ±16 ‰ in the boundary layer (1000 to 826 hPa), decreasing to ±10.5 ‰ at 750 to 681 hPa, and then increasing at higher altitudes due to uncertainty in the true profile above the aircraft ceiling. The TES V005 empirical error and estimated error are generally consistent with the observed spatial variability of HDO/H_2O. Future airborne measurements of HDO/H_2O above 5 km altitude, coordinated with TES observations, are highly desirable to provide information about the quality of the TES retrieval in the middle troposphere.

Acknowledgements. Thanks to B. Fisher for scheduling TES special observations. Support for R. Herman was provided by the NASA Aura Program. Participation by J. Cherry and J. Young was supported by the Jet Propulsion Laboratory (P.O. 1458171) and National Science Foundation EAGER Award Number ARC-1332274. Alaskan flights were supported by the National Science Foundation RAPID Award Number PLR-1342455. Thanks to Kirst Aviation and Arctic Aviation for their assistance in the data collection. The Alaskan aircraft Picarro water vapor unit was provide by NSF MRI (0976553) awarded to J. Welker. Part of the research described in this paper was carried out by the Jet Propulsion Laboratory, California Institute of Technology, under a contract with NASA.

References

Beer, R.: TES on the Aura Mission: scientific objectives, measurements and analysis overview, IEEE T. Geosci. Remote, 44, 1102–1105, 2006.

Beer, R., Bowman, K. W., Brown, P. D., Clough, S. A., Eldering, A., Goldman, A., Jacob, D. J., Lampel, M., Logan, J. A., Luo, M., Murcray, F. J., Osterman, G. B., Rider, D. M., Rinsland, C. P., Rodgers, C. D., Sander, S. P., Shepard, M., Sund, S., Ustinov, E. A., Worden, H. M., Worden, J., and Syvertson, M. (Eds.): Tropospheric Emission Spectrometer (TES) Level 2 Algorithm Theoretical Basis Document, V. 1.16, Jet Propulsion Laboratory, Pasadena, CA, JPL D-16474, 27 June 2002, available at: http://eospso.gsfc.nasa.gov/atbd-category/53 (last access: 7 December 2010), 2002.

Beer, R., Glavich, T. A., and Rider, D. M.: Tropospheric emission spectrometer for the Earth Observing System's Aura satellite, Appl. Optics, 40, 2356–2367, 2001.

Berden, G., Peeters, R., and Meijer, G.: Cavity ring-down spectroscopy: experimental schemes and applications, Int. Rev. Phys. Chem., 19, 565–607, doi:10.1080/014423500750040627, 2000.

Berkelhammer, M., Hu, J., Bailey, A., Noone, D., Still, C., Barnard, H., Gochis, D., Hsiao, G., Rahn, T., and Turnipseed, A.: The nocturnal water cycle in an open-canopy forest, J. Geophys. Res.-Atmos., 118, 10225–10242, doi:10.1002/jgrd.50701, 2013.

Bernath, P. F., McElroy, C. T., Abrams, M. C., Boone, C. D., Butler, M., Camy-Peyret, C., Carleer, M., Clerbaux, C., Coheur, P.-F., Colin, R., DeCola, P., DeMazière, M., Drummond, J. R., Dufour, D., Evans, W. F. J., Fast, H., Fussen, D., Gilbert, K., Jennings, D. E., Llewellyn, E. J., Lowe, R. P., Mahieu, E., McConnell, J. C., McHugh, M., McLeod, S. D., Michaud, R., Midwinter, C., Nassar, R., Nichitiu, F., Nowlan, C., Rinsland, C. P., Rochon, Y. J., Rowlands, N., Semeniuk, K., Simon, P., Skelton, R., Sloan, J. J., Soucy, M.-A., Strong, K., Tremblay, P., Turnbull, D., Walker, K. A., Walkty, I., Wardle, D. A., Wehrle, V., Zander, R., and Zou, J.: Atmospheric Chemistry Experiment (ACE): mission overview, Geophys. Res. Lett., 32, L15S01, doi:10.1029/2005GL022386, 2005.

Bowman, K. W., Worden, J., Steck, T., Worden, H. M., Clough, S., and Rodgers, C.: Capturing time and vertical variability of tropospheric ozone: a study using TES nadir retrievals, J. Geophys. Res.-Atmos., 107, 4723, doi:10.1029/2002JD002150, 2002.

Bowman, K. W., Rodgers, C. D., Kulawik, S. S., Worden, J., Sarkissian, E., Osterman, G., Steck, T., Luo, M., Eldering, A., Shephard, M. W., Worden, H., Lampel, M., Clough, S. A., Brown, P., Rinsland, C., Gunson, M., and Beer, R.: Tropospheric Emission Spectrometer: retrieval method and error analysis, IEEE T. Geosci. Remote, 44, 1297–1307, 2006.

Boxe, C. S., Worden, J. R., Bowman, K. W., Kulawik, S. S., Neu, J. L., Ford, W. C., Osterman, G. B., Herman, R. L., Eldering, A., Tarasick, D. W., Thompson, A. M., Doughty, D. C., Hoffmann, M. R., and Oltmans, S. J.: Validation of northern latitude Tropospheric Emission Spectrometer stare ozone profiles with ARC-IONS sondes during ARCTAS: sensitivity, bias and error analysis, Atmos. Chem. Phys., 10, 9901–9914, doi:10.5194/acp-10-9901-2010, 2010.

Brown, D., Worden, J., and Noone, D.: Comparison of atmospheric hydrology over convective continental regions using water vapor isotope measurements from space, J. Geophys. Res., 113, D15124, doi:10.1029/2007JD009676, 2008.

Craig, H.: Isotopic variations in meteoric waters, Science, 133, 1702–1703, doi:10.1126/science.133.3465.1702, 1961.

Dansgaard, W.: Stable isotopes in precipitation, Tellus, 16, 436–468, 1964.

Frankenberg, C., Yoshimura, K., Warneke, T., Aben, I., Butz, A., Deutscher, N., Griffith, D., Hase, F., Notholt, J., Schneider, M., Schrijver, H., and Röckmann, T.: Dynamic processes

AMTD
7, 3801–3833, 2014

Aircraft validation of TES HDO and H_2O

R. L. Herman et al.

governing lower-tropospheric HDO/H_2O ratios as observed from space and ground, Science, 325, 1374, doi:10.1126/science.1173791, 2009.
Gupta, P., Noone, D., Galewsky, J., Sweeny, C., and Vaughn, B. H.: Demonstration of high precision continuous measurements of water vapor isotopologues in laboratory and remote field deployments using WS-CRDS technology, Rapid Commun. Mass Sp., 23, 2534–2542, doi:10.1002/rcm.4100, 2009.
Herbin, H., Hurtmans, D., Turquety, S., Wespes, C., Barret, B., Hadji-Lazaro, J., Clerbaux, C., and Coheur, P.-F.: Global distributions of water vapour isotopologues retrieved from IMG/ADEOS data, Atmos. Chem. Phys., 7, 3957–3968, doi:10.5194/acp-7-3957-2007, 2007.
Herbin, H., Hurtmans, D., Clerbaux, C., Clarisse, L., and Coheur, P.-F.: $H_2{}^{16}O$ and HDO measurements with IASI/MetOp, Atmos. Chem. Phys., 9, 9433–9447, doi:10.5194/acp-9-9433-2009, 2009.
Herman, R. L. and Kulawik, S. S. (Eds.): Tropospheric Emission Spectrometer TES Level 2 (L2) Data User's Guide, D-38042, version 6.0, Jet Propulsion Laboratory, California Institute of Technology, Pasadena, CA, available at: http://tes.jpl.nasa.gov/documents (last access: 5 November 2013), 2013.
Herman, R. L. and Osterman, G. B. (Eds.): Tropospheric Emission Spectrometer Data Validation Report (Version F06_08, F06_09 data), D-33192, Version 5.0, Jet Propulsion Laboratory, California Institute of Technology, Pasadena, CA, available at: https://eosweb.larc.nasa.gov/project/tes/validation (last access: 9 April 2012), 2012.
Irion, F. W., Moyer, E. J., Gunson, M. R., Rinsland, C. P., Yung, Y. L., Michelsen, H. A., Salawitch, R. J., Chang, A. Y., Newchurch, M. J., Abbas, M. M., Abrams, M. C., and Zander, R.: Stratospheric observations of CH_3D and HDO from ATMOS infrared solar spectra: enrichments of deuterium in methane and implications for HD, Geophys. Res. Lett., 23, 2381–2384, 1996.
Kuang, Z., Toon, G. C., Wennberg, P. O., and Yung, Y. L.: Measured HDO/H_2O ratios across the tropical tropopause, Geophys. Res. Lett., 30, 1372, doi:10.1029/2003GL017023, 2003.
Kulawik, S. S., Worden, H., Osterman, G., Luo, M., Beer, R., Worden, J., Bowman, K., Eldering, A., Lampel, M., Steck, T., and Rodgers, C.: TES atmospheric profile retrieval characterization: an orbit of simulated observations, IEEE T. Geosci. Remote, 44, 1324, 2006.

Kulawik, S. S., Bowman, K. W., Luo, M., Rodgers, C. D., and Jourdain, L.: Impact of nonlinearity on changing the a priori of trace gas profile estimates from the Tropospheric Emission Spectrometer (TES), Atmos. Chem. Phys., 8, 3081–3092, doi:10.5194/acp-8-3081-2008, 2008.
Lacour, J.-L., Risi, C., Clarisse, L., Bony, S., Hurtmans, D., Clerbaux, C., and Coheur, P.-F.: Mid-tropospheric δD observations from IASI/MetOp at high spatial and temporal resolution, Atmos. Chem. Phys., 12, 10817–10832, doi:10.5194/acp-12-10817-2012, 2012.
Lee, J., Worden, J., Noone, D., Bowman, K., Eldering, A., LeGrande, A., Li, J.-L. F., Schmidt, G., and Sodemann, H.: Relating tropical ocean clouds to moist processes using water vapor isotope measurements, Atmos. Chem. Phys., 11, 741–752, doi:10.5194/acp-11-741-2011, 2011.
Lossow, S., Steinwagner, J., Urban, J., Dupuy, E., Boone, C. D., Kellmann, S., Linden, A., Kiefer, M., Grabowski, U., Glatthor, N., Höpfner, M., Röckmann, T., Murtagh, D. P., Walker, K. A., Bernath, P. F., von Clarmann, T., and Stiller, G. P.: Comparison of HDO measurements from Envisat/MIPAS with observations by Odin/SMR and SCISAT/ACE-FTS, Atmos. Meas. Tech., 4, 1855–1874, doi:10.5194/amt-4-1855-2011, 2011.
Moyer, E. J., Irion, F. W., Yung, Y. L., and Gunson, M. R.: ATMOS stratospheric deuterated water and implications for troposphere-stratosphere transport, Geophys. Res. Lett., 23, 2385–2388, 1996.
Murtagh, D., Frisk, U., Merino, F., Ridal, M., Jonsson, A., Stegman, J., Witt, G., Eriksson, P., Jiménez, C., Megie, G., de la Noë, J., Ricaud, P., Baron, P., Pardo, J. R., Hauchcorne, A., Llewellyn, E. J., Degenstein, D. A., Gattinger, R. L., Lloyd, N. D., Evans, W. F. J., McDade, I. C., Haley, C. S., Sioris, C., von Savigny, C., Solheim, B. H., McConnell, J. C., Strong, K., Richardson, E. H., Leppelmeier, G. W., Kyrölä, E., Auvinen, H., and Oikarinen, L.: An overview of the Odin atmospheric mission, Can. J. Phys., 80, 309–319, doi:10.1139/p01-157, 2002.
Noone, D.: Pairing measurements of the water vapor isotope ratio with humidity to deduce atmospheric moistening and dehydration in the tropical midtroposphere, J. Climate, 25, 4476–4494, 2012.
Noone, D., Galewsky, J., Sharp, Z. D., Worden, J., Barnes, J., Baer, D., Bailey, A., Brown, D. P., Christensen, L., Crosson, E., Dong, F., Hurley, J. V., Johnson, L. R., Strong, M., Toohey, D., Van Pelt, A., and Wright, J. S.: Properties of air mass mixing and humidity in the subtropics from measurements of the D/H isotope ratio of water vapor at the Mauna Loa Observatory, J. Geophys. Res.-Atmos., 116, D22113, doi:10.1029/2011JD015773, 2011.

O'Keefe, A. and Deacon, D. A. G.: Cavity ringdown optical spectrometer for absorption measurements using pulsed laser sources, Rev. Sci. Instrum., 59, 2544, doi:10.1063/1.1139895, 1988.

Pougatchev, N., August, T., Calbet, X., Hultberg, T., Oduleye, O., Schlüssel, P., Stiller, B., Germain, K. St., and Bingham, G.: IASI temperature and water vapor retrievals – error assessment and validation, Atmos. Chem. Phys., 9, 6453–6458, doi:10.5194/acp-9-6453-2009, 2009.

Randel, W. J., Moyer, E., Park, M., Jensen, E., Bernath, P., Walker, K., and Boone, C.: Global variations of HDO and HDO/H_2O ratios in the upper troposphere and lower stratosphere derived from ACE-FTS satellite measurements, J. Geophys. Res.-Atmos., 117, D06303, doi:10.1029/2011JD016632, 2012.

Rienecker, M. M., Suarez, M. J., Todling, R., Bacmeister, J., Takacs, L., Liu, H.-C., Gu, W., Sienkiewicz, M., Koster, R. D., Gelaro, R., and Stajner, I.: The GEOS-5 Data Assimilation System: a Documentation of GEOS-5.0 NASA TM 104606, 27, Technical Report Series on Global Modeling and Data Assimilation, 2007.

Rinsland, C. P., Gunson, M. R., Foster, J. C., Toth, R. A., Farmer, C. B., and Zander, R.: Stratospheric profiles of heavy water vapor isotopes and CH_3D from analysis of the ATMOS Spacelab 3 infrared solar spectra, J. Geophys. Res., 96, 1057–1068, 1991.

Rodgers, C. D.: Inverse Methods for Atmospheric Sounding: Theory and Practice, World Science, London, 2000.

Rodgers, C. D. and Connor, B. J.: Intercomparison of remote sounding instruments, J. Geophys. Res., 108, 4116, doi:10.1029/2002JD002299, 2003.

Schneider, M. and Hase, F.: Optimal estimation of tropospheric H_2O and δD with IASI/METOP, Atmos. Chem. Phys., 11, 11207–11220, doi:10.5194/acp-11-11207-2011, 2011.

Schneider, M., Hase, F., and Blumenstock, T.: Ground-based remote sensing of HDO/H_2O ratio profiles: introduction and validation of an innovative retrieval approach, Atmos. Chem. Phys., 6, 4705–4722, doi:10.5194/acp-6-4705-2006, 2006.

Schneider, M., Toon, G. C., Blavier, J.-F., Hase, F., and Leblanc, T.: H_2O and δD profiles remotely-sensed from ground in different spectral infrared regions, Atmos. Meas. Tech., 3, 1599–1613, doi:10.5194/amt-3-1599-2010, 2010.

Schoeberl, M. R., Douglass, A. R., Hilsenrath, E., Bhartia, P. K., Barnett, J., Beer, R., Waters, J., Gunson, M., Froidevaux, L., Gille, J., Levelt, P. F., and DeCola, P.: Overview of the EOS Aura Mission, IEEE T. Geosci. Remote, 44, 1066–1077, 2006.

Shephard, M. W., Herman, R. L., Fisher, B. M., Cady-Pereira, K. E., Clough, S. A., Payne, V. H., Whiteman, D. N., Comer, J. P., Vömel, H., Miloshevich, L. M., Forno, R., Adam, M., Osterman G. B., Eldering, A., Worden, J. R., Brown, L. R., Worden, H. M., Kulawik, S. S., Rider, D. M., Goldman, A., Beer, R., Bowman, K. W., Rodgers, C. D., Luo, M., Rinsland, C. P., Lampel, M., and Gunson, M. R.: Comparison of Tropospheric Emission Spectrometer (TES) water vapor retrievals with in situ measurements, J. Geophys. Res., 113, D15824, doi:10.1029/2007JD008822, 2008.

Steinwagner, J., Milz, M., von Clarmann, T., Glatthor, N., Grabowski, U., Höpfner, M., Stiller, G. P., and Röckmann, T.: HDO measurements with MIPAS, Atmos. Chem. Phys., 7, 2601–2615, doi:10.5194/acp-7-2601-2007, 2007.

Steinwagner, J., Fueglistaler, S., Stiller, G., von Clarmann, T., Kiefer, M., Borsboom, P. P., van Delden, A., and Rockmann, T.: Tropical dehydration processes constrained by the seasonality of stratospheric deuterated water, Nat. Geosci., 3, 262–266, 2010.

Tobin, C. D., Revercomb, H. E., Knuteson, R. O., Lesht, B. M., Strow, L. L., Hannon, S. E., Feltz, W. F., Moy, L. A., Fetzer, E. J., and Cress, T. S.: Atmospheric radiation measurement site atmospheric state best estimates for Atmospheric Infrared Sounder temperature and water vapor retrieval validations, J. Geophys. Res., 111, D09S14, doi:10.1029/2005JD006103, 2006.

Urban, J., Lautie, N., Murtagh, D., Eriksson, P., Kasai, Y., Lossow, S., Dupuy, E., de la Noe, J., Frisk, U., Olberg, M., Le Flochmoen, E., and Ricaud, P.: Global observations of middle atmospheric water vapour by the Odin satellite: an overview, Planet. Space Sci., 55, 1093–1102, doi:10.1016/j.pss.2006.11.021, 2007.

Worden, H. M., Logan, J. A., Worden, J. R., Beer, R., Bowman, K., Clough, S. A., Eldering, A., Fisher, B. M., Gunson, M. R., Herman, R. L., Kulawik, S. S., Lampel, M. C., Luo, M., Megretskaia, I. A., Osterman, G. B., and Shephard, M. W.: Comparisons of Tropospheric Emission Spectrometer (TES) ozone profiles to ozonesondes: methods and initial results, J. Geophys. Res., 112, D03309, doi:10.1029/2006JD007258, 2007.

Worden, J., Kulawik, S., Shephard, M., Clough, S., Worden, H., Bowman, K., and Goldman, A.: Predicted errors of Tropospheric Emission Spectrometer nadir retrievals from spectral window selection, J. Geophys. Res., 109, D09308, doi:10.1029/2004JD004522, 2004.

Worden, J., Bowman, K., Noone, D., Beer, R., Clough, S., Eldering, A., Fisher, B., Goldman, A., Gunson, M., Herman, R., Kulawik, S. S., Lampel, M., Luo, M., Osterman, G., Rinsland, C., Rodgers, C., Sander, S., Shephard, M., and Worden, H.: Tropospheric Emission Spectrome-

AMTD
7, 3801–3833, 2014

Aircraft validation of TES HDO and H_2O

R. L. Herman et al.

ter observations of the tropospheric HDO/H_2O ratio: estimation approach and characterization, J. Geophys. Res., 111, D16309, doi:10.1029/2005JD006606, 2006.
Worden, J., Noone, D., Galewsky, J., Bailey, A., Bowman, K., Brown, D., Hurley, J., Kulawik, S., Lee, J., and Strong, M.: Estimate of bias in Aura TES HDO/H_2O profiles from comparison of TES and in situ HDO/H_2O measurements at the Mauna Loa observatory, Atmos. Chem. Phys., 11, 4491–4503, doi:10.5194/acp-11-4491-2011, 2011.
Worden, J., Kulawik, S., Frankenberg, C., Payne, V., Bowman, K., Cady-Peirara, K., Wecht, K., Lee, J.-E., and Noone, D.: Profiles of CH_4, HDO, H_2O, and N_2O with improved lower tropospheric vertical resolution from Aura TES radiances, Atmos. Meas. Tech., 5, 397–411, doi:10.5194/amt-5-397-2012, 2012.
Zakharov, V. I., Imasu, R., Gribanov, K. G., Hoffmann, G., and Jouzel, J.: Latitudinal distribution of the deuterium to hydrogen ratio in the atmospheric water vapor retrieved from IMG/ADEOS data, Geophys. Res. Lett., 31, L12104, doi:10.1029/2004GL019433, 2004.
Zhu, Y. and Gelaro, R.: Observation sensitivity calculations using the adjoint of the Gridpoint Statistical Interpolation (GSI) analysis system, Mon. Weather Rev., 136, 335–351, doi:10.1175/MWR3525.1, 2008.

AMTD
7, 3801–3833, 2014

Aircraft validation of TES HDO and H_2O

R. L. Herman et al.

Table 1. Summary of aircraft flights and collocated Aura TES special observations over the Alaskan interior boreal forest near 64.5° N, 148° W. Average cloud estimated optical depth (OD) is from the nearest TES retrieval. The number of TES scans that have good quality, DOFS > 1.1, and spatially overlap the aircraft flight path are shown in the "Good scans" column. The height of the boundary layer, Z_{BL}, is defined here as the level at which water vapor drops 10 % below the boundary layer mean value. Boundary layer mean water vapor, $\langle H_2O \rangle$, and δD, $\langle \delta D \rangle$, are measured by a Picarro Isotopic Water Analyzer onboard the Cessna aircraft. Two of these aircraft flights (27 August 2011 and 12 July 2013) did not have coincident TES special observations.

Date	Runid	CloudOD (TES)	Overlapping Good scans (TES)	Aircraft Ceiling (km)	Aircraft BL $\langle H_2O \rangle$ (ppt)	Aircraft BL Z_{BL} (km)	Aircraft BL $\langle \delta D \rangle$ (‰)
26 Jul 2011	13 182	2	14	4.6	~ 12.5	2.0	−228 ± 11
27 Aug 2011	NA	< 0.1	NA	3.9	10.4	1.2	−234 ± 10
12 Jul 2012	15 046	1	8, 10, 11, 12	4.0	~ 7.5	2.0	−253 ± 5
28 Jul 2012	15 143	< 0.1	10, 11, 12	4.4	11.8 ± 0.3	1.5	−214 ± 2
6 Aug 2012	15 206	0.1	8, 9, 10, 11, 12	4.1	9.2 ± 0.6	1.9	−222 ± 10
15 Aug 2012	15 266	< 0.5	8, 11, 12	4.2	7.6 ± 0.3	2.0	−215 ± 4
12 Jul 2013	NA	NA	NA	3.1	10.5 ± 0.2	1.7	−239 ± 13

AMTD
7, 3801–3833, 2014

Aircraft validation of TES HDO and H_2O

R. L. Herman et al.

Table 2. Aircraft measurement statistics of atmospheric water vapor δD variability over the Alaskan interior boreal forest. The data are binned by TES pressure level. Aircraft ascent data only are used.

Pressure (hPa)	Mean δD (‰)	St. Dev. δD (‰)	Number of data points
1000.00	−224.1	15.9	647
908.514	−231.6	16.3	1387
825.402	−235.3	21.1	930
749.893	−261.6	30.6	885
681.291	−276.1	27.7	628
618.966	−305.2	20.1	557
562.342	−300.4	5.1	75

AMTD
7, 3801–3833, 2014

Table 3. Aura TES statistics of atmospheric water vapor δD variability over the Alaskan interior boreal forest. Twenty seven TES transect special observations from July–August 2011 and July–August 2012 are binned together by pressure level (DOFS > 1.1) for mean δD and standard deviation of δD.

TES Pressure (hPa)	Mean δD (‰)	St. Dev. δD (‰)
1000.66	−108.4	25.9
908.514	−163.0	35.2
825.562	−218.9	32.5
749.893	−254.4	27.2
681.291	−282.0	23.1
618.966	−316.7	25.7
562.342	−337.3	26.9
510.898	−357.1	29.6
464.160	−361.2	28.3
421.698	−365.1	27.9
383.117	−369.7	23.8
348.069	−374.1	20.1
316.227	−389.7	15.3
287.298	−404.9	10.7
261.016	−432.6	7.4
237.137	−459.0	4.4
215.444	−494.8	3.2
195.735	−528.2	2.2
177.829	−559.5	1.3

AMTD
7, 3801–3833, 2014

Table 4. Error budget for Aura TES V005 δD. Error terms are shown for both the boundary layer (1000 to 826 hPa) and the free troposphere up to the aircraft ceiling (750 to 562 hPa). The aircraft variability comes from seven aircraft flights over the Alaskan interior boreal forest (see Table 1 and Sect. 4.1). The scan-to-scan TES variability includes 27 TES transects and 253 scans of good quality (see Sect. 4.1). The TES V005 bias is calculated to minimize the differences between TES and aircraft with averaging kernel applied for 16 matches (see Sect. 4.3). The sensitivity to assumptions about the true profile above the aircraft ceiling is adapted from Fig. 5 (Sect. 4.4). The TES empirical error is calculated from the 16 good TES-aircraft matches, Eq. (7). The TES estimated error is shown here only for the 28 Jul 2012 TES special observation, but is typical.

Parameter	Boundary Layer	Free Troposphere
Aircraft variability (1 – σ st. dev.)	±16 ‰	±30 ‰
Scan-to-scan TES variability (1 – σ st. dev.)	±34.1 ‰	±26.5 ‰
TES V005 bias	+98 ‰	+37 ‰
Sensitivity to "true" above aircraft	±5 ‰ (approx.)	±20 ‰
TES empirical error	±26 ‰	±22 ‰
TES estimated error (28 Jul 2012)	±16 ‰	±10.5 ‰ (up to 681 hPa)

AMTD
7, 3801–3833, 2014

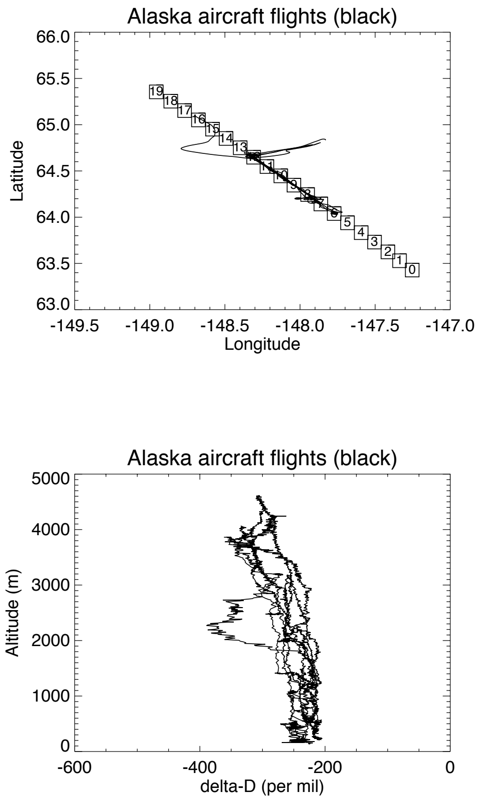

Fig. 1. Aircraft path (top) and profiles (bottom) of water vapor δD from seven flights over the Alaskan interior boreal forest. Superimposed on the aircraft latitude and longitude are the geolocations of the TES transect special observation (scans labeled 0 through 19). The largest excursion in delta-D at 2000 m altitude was measured during the 12 July 2013 flight, a layer of depleted air observed both on aircraft ascent and descent in the free troposphere above the top of a well-defined boundary layer.

AMTD
7, 3801–3833, 2014

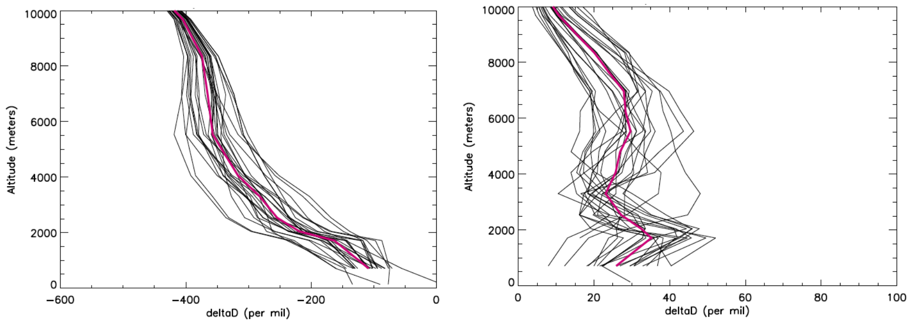

Fig. 2. (Left) Mean water vapor δD from each of 27 TES transect special observations (thin black lines) and the overall mean profile (thick red line) over the Alaskan interior boreal forest in July and August 2011, and July and August 2012. (Right) The standard deviation of water vapor δD from each of the same 27 TES transect special observations (thin black lines) and the overall mean profile (thick red line). The values of the overall mean and standard deviation are also listed in Table 3.

AMTD
7, 3801–3833, 2014

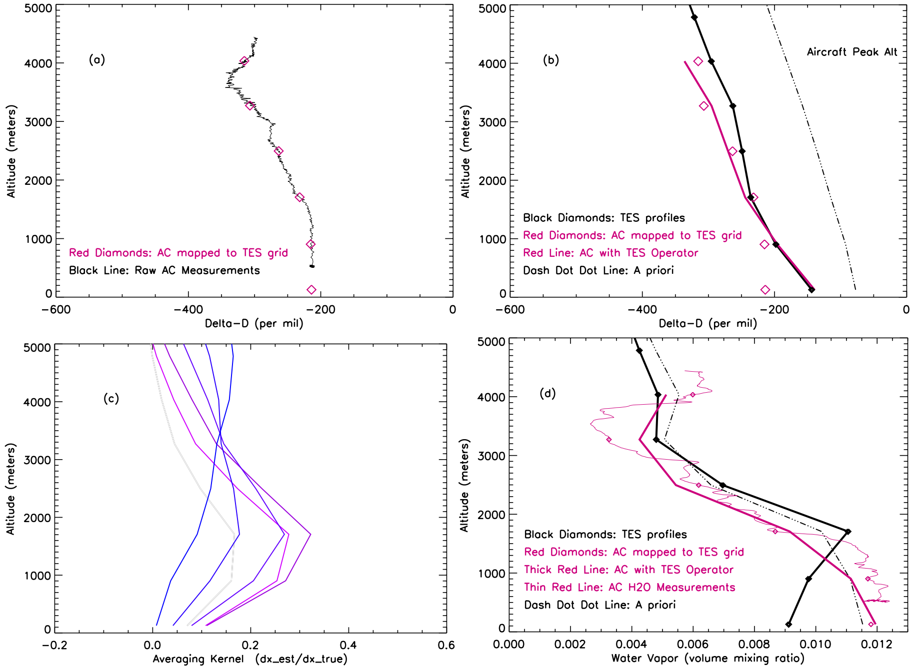

Fig. 3. Comparison of the δD tropospheric profile from the Alaskan interior boreal forest aircraft flight of 28 July 2012 with the coincident TES retrieval (run 15 143, scan 12). **(a)** Raw aircraft ascent δD (black line) and aircraft values interpolated to TES levels (red diamonds); **(b)** δD profiles of the tropical prior (dash dot dot line), aircraft interpolated to TES levels (red diamonds), aircraft with TES operator (red line), and the TES retrieval (black line); **(c)** TES HDO averaging kernels for these lowest levels of the atmosphere; **(d)** H_2O profiles of the tropical prior (dash dot dot line), aircraft interpolated to TES levels (red diamonds), aircraft with TES operator (red line), and the TES retrieval (black line).

AMTD
7, 3801–3833, 2014

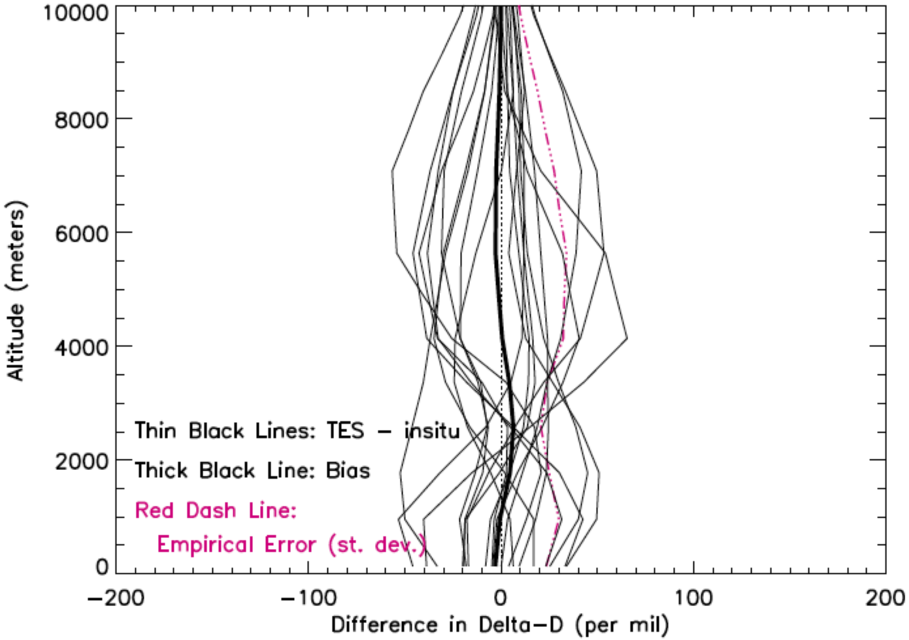

Fig. 4. Comparisons of TES δD minus aircraft δD with averaging kernel applied for the 16 scans that have good quality, DOFS > 1.1, and spatially overlap the aircraft flight path (see Table 1). Also plotted are the TES bias (thick black line) and standard deviation (dashed red line). In this figure TES HDO has been corrected by $\boldsymbol{\delta}_{\text{bias}}$ (Eq. 3).

AMTD
7, 3801–3833, 2014

Title Page
Abstract | Introduction
Conclusions | References
Tables | Figures
◀I | ▶I
◀ | ▶
Back | Close
Full Screen / Esc
Printer-friendly Version
Interactive Discussion

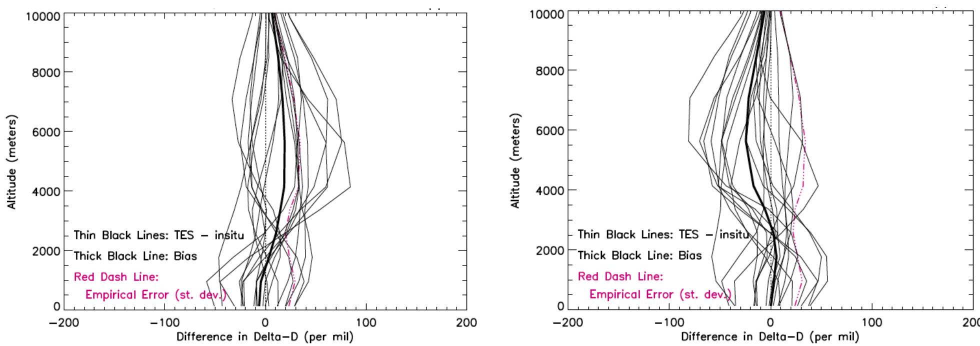

Fig. 5. Sensitivity of TES δD minus "true" δD for different assumptions above the level of the aircraft measurements. Scans and constraints are the same as for the best estimate of the true in Fig. 4. (left) Comparison in which the "true" δD is aircraft data, with scaled prior minus 30 ‰ above the aircraft. (right) Comparison in which the "true" δD is aircraft data, with scaled prior plus 30 ‰ above the aircraft.

AMTD
7, 3801–3833, 2014

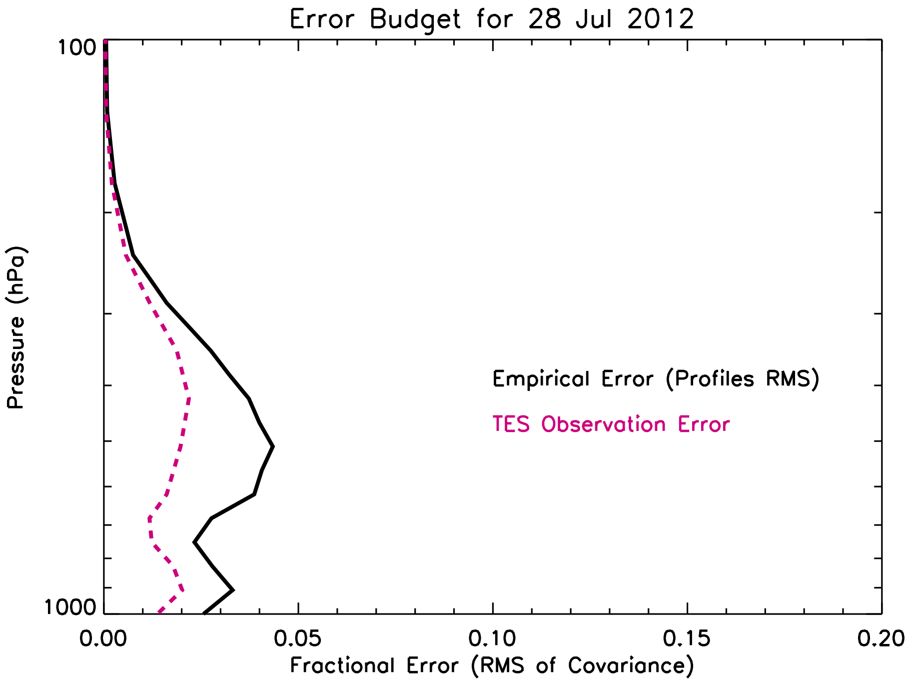

Fig. 6. Error analysis for the TES-aircraft coincident observations on 28 July 2012 over the Alaskan interior boreal forest. The red dashed line is the fractional estimated error based on the TES HDO/H_2O observation error. The solid black line is the empirical error of TES HDO/H_2O from Eq. (7).

AMTD
7, 3801–3833, 2014